Precision measurements of the radio emission in air showers with LOFAR

J.R. Hörandel[*,†], S. Buitink[*], A.Corstanje[*], J.E. Enriquez[*], H. Falcke[*,**], A. Nelles[*,†], J.P. Rachen[*], S. Thoudam[*], P. Schellart[*], O. Scholten[‡], S. ter Veen[*], T.N.G. Trinh[‡] and The LOFAR Collaboration[**]

[*]*Department of Astrophysics/IMAPP, Radboud University Nijmegen, P.O. Box 9010, 6500 GL Nijmegen, The Netherlands*
[†]*Nikhef, Science Park Amsterdam, 1098 XG Amsterdam, The Netherlands*
[**]*Netherlands Institute for Radio Astronomy (ASTRON), Postbus 2, 7990 AA Dwingeloo, The Netherlands*
[‡]*KVI-CART, University of Groningen, P.O. Box 72, 9700 AB Groningen, The Netherlands*

Abstract. The LOFAR radio telescope is used to observe radio emission from extensive air showers. In the last year we have achieved a major break through in measuring the properties of cosmic rays with the radio technique. In these proceedings, recent results from LOFAR will be reviewed.

Keywords: Cosmic rays, air showers, radio emission, LOFAR
PACS: 96.50.sd, 95.55.Jz

INTRODUCTION

To understand the origin of high-energy cosmic rays is one of the open key questions in astroparticle physics [1, 2]. An inspiring article, published in 2003 [3] triggered the renaissance of radio detection of extensive air showers with the ultimate goal to measure the properties of cosmic rays with this technique and the pioneer experiments LOPES [4] and CODALEMA [5] have been initiated. The big success of these pathfinders stimulated further investigations of the radio emission of air showers on larger scales, such as Tunka-Rex, AERA at the Pierre Auger Observatory and the LOFAR radio telescope [6]. Significant progress has been achieved in the last decade [7] and we now understand the emission processes of the radio waves in the atmosphere. Most of the emission is due to the interaction of the shower with the magnetic field of the Earth, which leads to a transverse current in the shower. In addition to this emission, the overabundance of electrons in the shower that are collected from atmospheric molecules leads to a current in the direction of the shower.

In this article, we will give an overview on recent activities of the LOFAR key science project Cosmic Rays [8].

EXPERIMENTAL SET-UP

LOFAR is a distributed radio telescope [6]. Its antennas are located in different countries in northern Europe with the densest concentration in the north of the Netherlands, in the Province of Drenthe. The antennas of LOFAR are grouped into *stations*. A station consist of a number of low-band antennas ($10-90$ MHz) and high-band antennas ($110-240$ MHz). The 24 stations within the ~ 2 km wide core are distributed in an irregular pattern that maximizes *uv*-coverage, or spatial frequencies for standard interferometric observations. Core stations and remote stations consist of 96 low-band antennas plus 48 high-band antennas. International stations have 96 low-band antennas and 96 high-band antennas. At the center of the LOFAR core six stations are located in a roughly 320 m diameter area, called the *Superterp*, providing both the shortest baselines for interferometric observations and the densest population of antennas ideal for cosmic-ray observations.

While every LOFAR station is equipped with the necessary electronics to observe cosmic rays, the current data set is taken with the central 24 stations, where additional information from particle detectors is available. The core of LOFAR is depicted in Fig. 1. For comparison, other major set-ups to detect radio emission from air showers are shown as well, namely LOPES [4], Tunka-Rex [9], and AERA at the Pierre Auger Observatory [10].

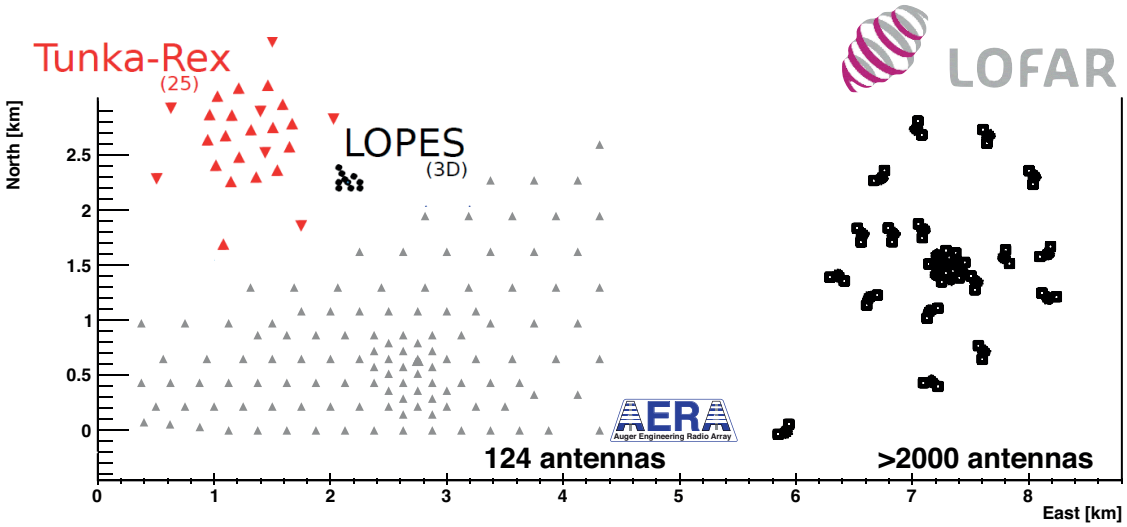

FIGURE 1. Schematic view of major radio detectors to measure cosmic rays. The core of LOFAR is compared to other set-ups (LOPES [4], Tunka-Rex [9], and AERA at the Pierre Auger Observatory [10]). (Figure adapted from A. Haungs)

The low-band antennas are the main tool for cosmic-ray detection. A low-band antenna consists of two orthogonal inverted V-shaped dipoles, each with a length of 1.38 m. These are supported by a central polyvinyl chloride pole, which holds the low-noise amplifier and guides the signal cables. The dipoles X and Y, that make up each antenna, are oriented southwest to northeast (SW-NE) and southeast to northwest (SE-NW). The low-noise amplifier has an intentional impedance mismatch with the antenna. This mismatch, combined with the characteristic length of the dipoles, makes the system sensitive in a broad band from $10-90$ MHz. For most observations the frequency range is limited by a combination of selectable hardware and software filters to $30-80$ MHz to suppress strong Radio Frequency Interference (RFI) in the outer bands. The low-band antennas are designed to be sky noise limited after RFI has been removed.

The high-band antennas have been optimized for a frequency band of $110-240$ MHz. The design clusters 16 antenna elements into a *tile*, the signals from these elements are amplified and combined in an analog beam-former. This means that while the low-band antennas are sensitive to the whole sky the high-band antennas are most sensitive within the $\sim 20^\circ$ of the tile-beam, of which the direction is chosen at the start of every observation. This results in a smaller effective area for cosmic-ray observations, as the measurement will only be optimal if the direction of the cosmic ray happens to coincide with the beam direction of the particular observation.

For all types of antennas, there is a possibility to store a snapshot of the original data. Every station is equipped with ring-buffers, the so called Transient Buffer Boards (TBBs). These continuously store the last 5 s of data. When triggered, the contents of the TBBs are frozen, read out via the Wide Area Network and stored on disk for further analysis. The trigger can be generated based on various parameters in an FPGA at the local receiver unit.

Alternatively, the trigger can be generated by an array of particle detectors or received from outside of LOFAR. Currently, the main trigger for cosmic-ray observation is provided by the particle detectors of LORA. LORA, the LOFAR Radboud Air Shower Array, is an array of particle detectors co-located with the center of LOFAR. The array provides a reconstruction of basic parameters of recorded air showers, such as the direction and the position of impact, as well as the energy of the incoming cosmic ray [11]. Conditions at which triggers are sent to LOFAR can be adjusted to match the desired energy threshold. Requiring triggers in 13 detectors out of the 20 yields a threshold energy of $2.4 \cdot 10^{16}$ eV, with an average trigger rate of 0.8 events/hour.

For future observations, a radio self-trigger will be implemented, using the current dataset as a training set to deduce trigger criteria. Using every LOFAR station individually will dramatically increase the effective area. Essential for measuring cosmic rays with LOFAR as a radio telescope is that the whole process of triggering and storing radio pulse data can take place without interfering with the ongoing observations.

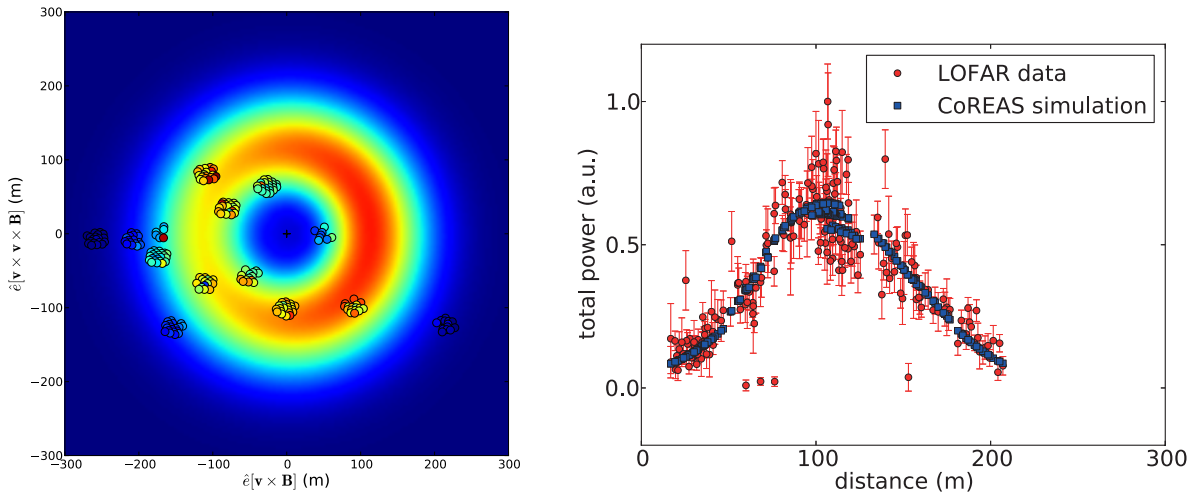

FIGURE 2. Radio emission from extensive air showers in the frequency range 110 – 190 MHz [12]. Footprint of a measured shower (*left*) and the radio power as a function of the distance to the shower axis (*right*), measured values (red) are compared to predictions of CoREAS (blue).

MEASURING A CHERENKOV RING AT FREQUENCIES ABOVE 100 MHZ

The high antenna density of LOFAR enables detailed studies of the radiation pattern generated by individual showers [12]. This is very instructive due to the intrinsic asymmetry of the signal which hinders averaging over showers. LOFAR is the only current experiment that can test theoretical predictions about the signal pattern in individual air showers.

Using these single air showers several approaches how to extract information from the radio pattern about the characteristics of the air shower are tested. The measured patterns are in their full extend compared to Monte Carlo simulations as shown in figure Fig. 2 (*left*). This illustrates to what extend the current air shower simulations capture the measured features and how this contains information about the shower development. Furthermore, the measured showers show the predicted ring structures and these are used to extract the ring size. The precision that can be obtained for the ring size determines the accuracy of measurement of the depth of the shower maximum.

As shown in [13] the simulation code CoREAS [14] describes the data from the low-band antennas well and in great detail. With these simulations it can be illustrated what is expected from an observation at higher frequencies. For a single event, the predicted power as a function of the distance to the shower axis is depicted in Fig. 2 (*right*) together with measured values. The ring-like structure emerges as an enhancement at around 100 m. From these data the ring size can be determined to an accuracy of about 15 m. Further details are given in Ref. [12].

THE SHAPE OF THE RADIO WAVEFRONT

The high density of antennas is also very useful to study the precise shape of the radio wavefront in detail [15]. Assuming a point source would result in a spherical wavefront shape, which is used for analysis of LOPES data [16]. It is argued in [17] that the actual shape of the wavefront is not spherical, but rather conical, as the emission is not point-like but stretched along the shower axis. In a recent further refinement of this study, based on CoREAS simulations, evidence is found for a hyperbolic wavefront shape (spherical near the shower axis, and conical further out) [18]. However, due to high ambient noise levels, the timing precision of these measurements did not allow for a distinction between spherical, hyperbolical, and conical shapes on a shower-by-shower basis, and only on average a hyperbolic wavefront shape has been favored. We use the LOFAR measurements to clarify this question.

We fitted a sphere, a cone, and a hyperboloid to the LOFAR measurements of the arrival time of the wavefront in each antenna. The procedure is illustrated in Figs. 3 and 4. The figures show the arrival time (in the shower plane) as a function of the distance to the shower axis. Data of the same shower are fitted with a sphere (Fig. 3, *left*), a cone (Fig. 3, *right*), and a hyperboloid (Fig. 4, *left*). The lower part of the plots illustrate the residuals with respect to the fit.

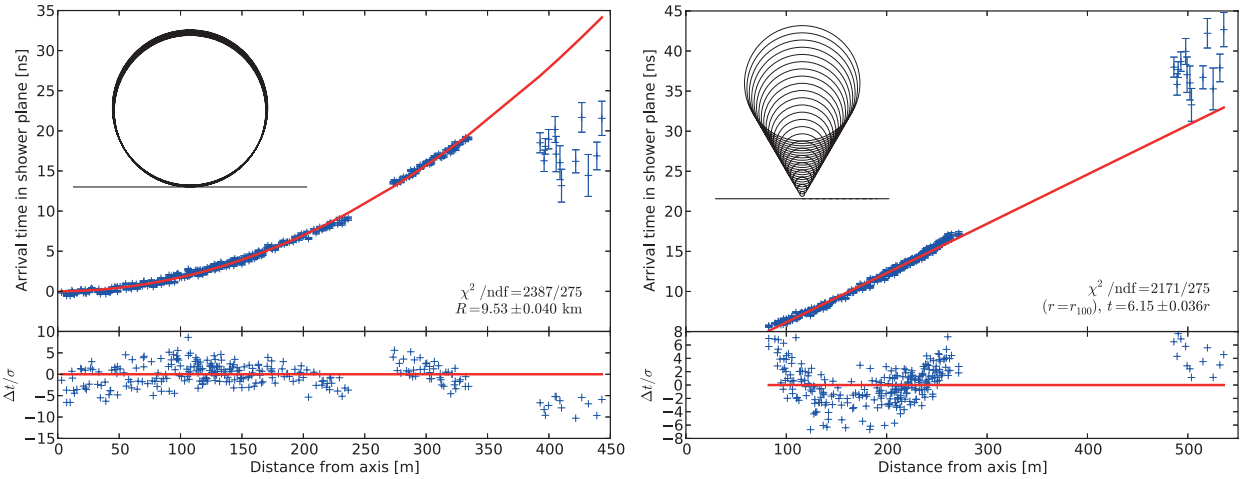

FIGURE 3. The arrival time differences from a plane wave as a function of distance to the shower axis with the best fitting shape solutions. A spherical (*left*), a conical (*right*), and a hyperbolical (Fig. 4, *left*) fit has been applied, respectively. Each plot shows the arrival times as a function of the distance to the shower axis (top panel) and deviations from the best fit scaled to the uncertainty for each data point (bottom panel). Note that the shower core position is a free parameter in each fit, therefore the positions of the data points on the abscissa differ between fits, as is in particular evident for the spherical fit.[15].

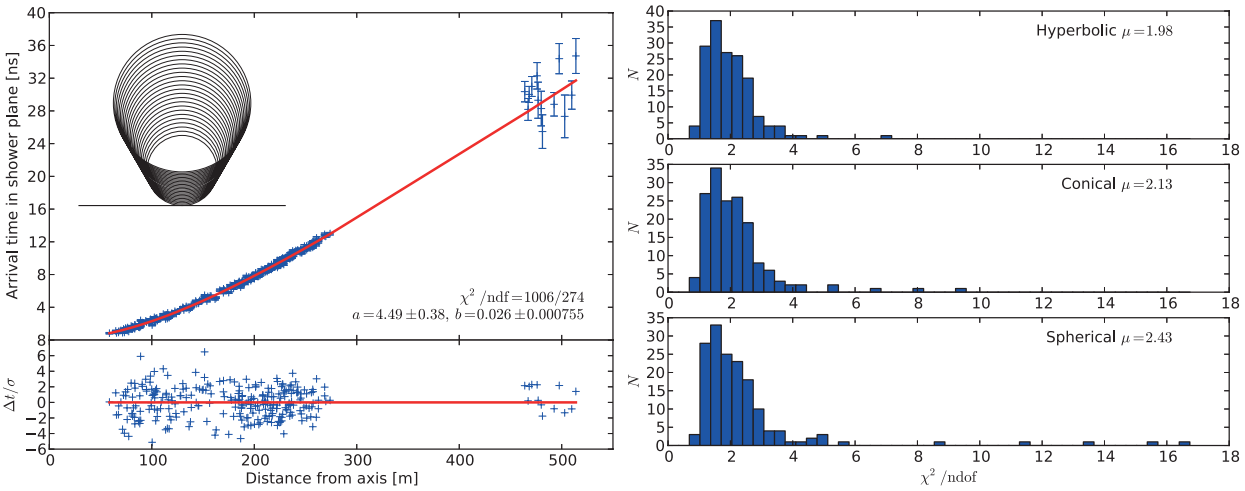

FIGURE 4. *Left*: same as Fig. 3 for a hyperbolical fit. *Right*: Fit quality for a hyperbolic (top), conical (middle), and spherical (bottom) wavefront shape [15].

The wavefront shape of this air shower is best fitted by a hyperbola due to significant curvature near the shower axis. The shower core position, left as free parameters in the fitting procedure, is significantly different for the three fits, see Ref. [15].

The χ^2/ndf values obtained for all showers are depicted in Fig. 4 (*right*). From these distributions it is not immediately evident which wavefront shape (if any) is favored. However, these distributions do not reflect the often significant differences in fit quality for a single shower. Furthermore, even if the wavefront shape were always hyperbolic one would still expect to see shapes that appear conical or spherical for individual showers, depending on the shower geometry and the part of the shower front that is sampled by the detector.

In order to check which wavefront shape is favored by the overall dataset we perform a likelihood ratio test. The test statistic for the conical case is:

$$D = -2\,\frac{\ln(\text{likelihood hyperbolic})}{\ln(\text{likelihood conical})} = \sum_{k}^{N} \chi^2_{\text{con}} - \chi^2_{\text{hyp}} \tag{1}$$

where the sum k is over all N showers. For an appropriate choice of parameters the hyperbolic function can turn into either a conical or a spherical function. Thus, the solution space of the spherical and conical fit functions are subsets of the solution space of the hyperbolic fit. Therefore (if the fit converged correctly) the hyperbolic fit will always have a lower χ^2/ndf value, even when the wavefront shape is intrinsically spherical or conical.

Under the null hypothesis that the wavefront shape is intrinsically conical (or spherical) the test statistic D should follow a $\chi^2(N)$ distribution. For large N, the $\chi^2(N)$ distribution approximates a Gaussian with mean N and standard deviation $\sqrt{2N} \ll D-N$. From the data we obtain the value $D = 6309$. The probability for this value to occur if the shape is conical is effectively zero, $p \ll 10^{-9}$, as the D-value is very far out of the distribution range.

There are two possible reasons for obtaining a higher value. Either the timing uncertainties are underestimated or the wavefront shape is generally not conical. Given the obtained reduced χ^2 values of the hyperbolic fit, averaging to 1.98, it is unlikely that the uncertainties are underestimated by more than a factor ~ 1.5. This is not enough by far to explain the measured value of the test statistic. Therefore we reject the null hypothesis that the wavefront shape is conical. Using the same procedure we also reject a spherical wavefront shape, with $D = 16927$ and correspondingly an even (much) lower p-value. Moreover, the lack of overall structure in the residuals of the hyperbolic fits (at our timing precision) argues against a more complicated wavefront shape. Therefore we conclude that the wavefront shape is hyperbolic. Furthermore, we do not see any evidence for a deviation from rotational symmetry (around the shower axis). So this is either not present, or is not resolvable with the current timing resolution.

LOFAR KEY FINDINGS

The LOFAR key science project Cosmic Rays has made tremendous progress in detecting radio emission from extensive air showers in the last year, taking advantage of the high antenna density in the LOFAR core, the large frequency coverage $10-240$ MHz, and the time resolution of better than 1 ns. We now have a quantitative description of the emission processes in the atmosphere and are able to determine the properties of cosmic rays (arrival direction, energy, mass/type of particle) from the radio observations. In particular, the following key findings have been achieved:

Lateral distribution function. An analytical description has been found for the signal distribution of the radio emission from air showers at ground level [19, 20]. The shape of the signal distribution is not rotational symmetric and can be parameterized as

$$P(x',y') = A_+ \cdot \exp\left(\frac{-[(x'-X_c)^2+(y'-Y_c)^2]}{\sigma_+^2}\right) - C_0 \cdot A_+ \cdot \exp\left(\frac{-[(x'-(X_c+x_-))^2+((y'-Y_c))^2]}{(C_1 \cdot e^{C_2 \cdot \sigma_+})^2}\right). \quad (2)$$

With the parameters A_+, σ_+, X_c, Y_c and x_-. The constants C_0, C_1 and C_2 can be determined from simulations. All remaining parameters can be reduced to physical parameters, namely the energy E of the air shower, the depth of the shower maximum X_{max}, the position of the shower axis (X,Y) and the arrival direction (θ,ϕ).

Cherenkov ring in the 100 MHz regime. The data of air showers collected with the LOFAR high-band antennas provide unprecedented detailed measurements of radio emission in the frequency range $110-230$ MHz [12]. For the first time, we measure a dominant relativistic time compression of the radio emission of air showers on a single-event basis. We show that it is possible to measure the radius of this Cherenkov ring with an accuracy of less than 20 m. This is sufficient to give an indication of the depth of the shower maximum.

Shape of the radio wavefront. We have shown that the wavefront of the radio emission in extensive air showers is measured to a high precision (better than 1 ns for each antenna) with the LOFAR radio telescope [15]. The shape of the wavefront is best parameterized as a hyperboloid, curved near the shower axis and approximately conical further out. A hyperbolic shape fits significantly better than the previously proposed spherical and conical shapes. Reconstruction of the shower geometry using a hyperbolic wavefront yields a more precise determination of the the shower direction, and an independent measurement of the core position. Assuming the resulting reconstructed direction has no systematic bias, the angular resolution improves from $\sim 1^\circ$ (planar wavefront) to $\sim 0.1^\circ$ (hyperbolic).

Polarization and emission mechanisms. The measured radio emission from extensive air showers is strongly polarized, with a median degree of polarization of nearly 99% [21, 22]. In all measured air showers the geomagnetic emission mechanism clearly dominates the polarization pattern. However, a sub-dominant charge-excess component

can also be seen, varying in strength between showers. The relative strength of both contributions is quantified by the charge-excess fraction. We find that the measured charge-excess fraction is higher for air showers arriving from closer to zenith. Furthermore, the measured charge-excess fraction also increases with increasing observer distance from the air shower symmetry axis. The measured values range from $(3.3 \pm 1.0)\%$ for very inclined air showers at 25 m from the shower axis to $(20.3 \pm 1.3)\%$ for almost vertical showers at a distance of 225 m to the shower axis.

Properties of cosmic rays. Fitting a hyperboloid to the radio shower front, we can reconstruct the **arrival direction** with an accuracy of 0.1°. The **energy** of the incoming cosmic ray can be determined by fitting the two-dimensional LDF to the measured radio signals with an uncertainty of the order of 30%. We have developed a new method to reconstruct the atmospheric **depth of the shower maximum** X_{max} with radio measurements [23, 24]. It is based on the complete two-dimensional distribution of the emitted radio power which strongly depends on the longitudinal development of the shower. Application of the technique to LOFAR data yields very accurate reconstructions of typically 17 g/cm^2.

In summary, looking at the results from LOFAR, but also from the other experiments, it became clear during the 2014 ARENA symposium that the radio detection of air showers has reached maturity. It can now be used to study the properties of cosmic rays. In particular, this makes LOFAR an excellent observatory to study the cosmic-ray composition in the energy regime of $10^{17} - 10^{18}$ eV, which may harbor the transition from a Galactic to extragalactic origin.

ACKNOWLEDGMENTS

We acknowledge financial support from NOVA, SNN, FOM, as well as from NWO, VENI grant 639-041-130. We acknowledge funding from the European Research Council (FP/2007-2013) / ERC Grant Agreement n. 227610.

LOFAR, the Low Frequency Array designed and constructed by ASTRON, has facilities in several countries, that are owned by various parties (each with their own funding sources), and that are collectively operated by the International LOFAR Telescope foundation under a joint scientific policy.

REFERENCES

1. J. Blümer, R. Engel, and J. Hörandel, *Prog. Part. Nucl. Phys.* **63**, 293 (2009).
2. M. Nagano and A. Watson, *Rev. Mod. Phys.* **72**, 689 (2000).
3. H. Falcke and P. Gorham, *Astropart. Phys.* **19**, 477 (2003),
4. H. Falcke et al., *Nature* **435**, 313 (2005).
5. O. Ravel et al., *Nucl. Instrum. Meth.* **A518**, 213 (2004).
6. M. van Haarlem et al., *Astron.Astrophys.* **556**, A2 (2013).
7. T. Huege, *Braz.J.Phys.* **44**, 520 (2014).
8. P. Schellart et al., *Astron.Astrophys.* **560**, A98 (2013).
9. D. Kostunin et al., *Nucl.Instrum.Meth.* **A742**, 89 (2014).
10. J. Neuser for the Pierre Auger Collaboration, these proceedings (2014).
11. S. Thoudam et al., *Nucl.Instrum.Meth.* **A767**, 339 (2014).
12. A. Nelles et al., Measuring a Cherenkov ring in the radio emission from air showers at 110-190 MHz with LOFAR, submitted to Astroparticle Physics (2014).
13. S. Buitink for the LOFAR Collaboration, "Shower Xmax determination based on LOFAR radio measurements," in *Proceedings of the 33rd International Cosmic Ray Conference*, 2013.
14. T. Huege, M. Ludwig, and C. W. James, *ARENA 2012, AIP Conf. Proc. 1535* pp. 128 (2013).
15. A. Corstanje et al. (2014), arXiv:1404.3907.
16. A. Nigl et al. LOPES collaboration, *Astronomy & Astrophysics* **487**, 781 (2008).
17. F. G. Schröder et al. LOPES collaboration, "Investigation of the Radio Wavefront of Air Showers with LOPES and REAS3," in *International Cosmic Ray Conference*, 2011, vol. 3 of *International Cosmic Ray Conference*, p. 64.
18. W. D. Apel et al. LOPES collaboration, *to be published in JCAP,* (2014), arXiv:1404.3283.
19. A. Nelles et al., *Astropart.Phys.* **60**, 13 (2015).
20. A. Nelles et al., these proceedings (2014).
21. P. Schellart, et al. (2014), arXiv:1406.1355.
22. O. Scholten et al., these proceedings (2014).
23. S. Buitink et al. (2014), arXiv:1408.7001.
24. S. Buitink et al., these proceedings (2014).